Peer-reviewed Statement

Spatial Patterns of Glacier Meltwater and Mountain Wetland Connectivity in the Peruvian Andes

By D. Xuan, R. Becker, M. Vargas Valverde, B. Davies, J. C. Ely, O. King, N. Montoya, C. Onof, A. C. Ross, W. Buytaert.

This is a non-reviewed preprint submitted to EarthArXiv. Subsequent versions may have slightly different content after peer review.

Spatial Patterns of Glacier Meltwater and Mountain Wetland Connectivity in the Peruvian Andes

D. Xuan [1], R. Becker [1], M. Vargas Valverde [2], B. Davies [3], J. C. Ely [4], O. King [3], N. Montoya [2], C. Onof [1], A. C. Ross [1], W. Buytaert [1]

[1]Department of Civil and Environmental Engineering, Imperial College London, United Kingdom
[2]Departamento Académico de Agricultura, Universidad Nacional de San Antonio Abad del Cusco (UNSAAC), Cusco, Peru
[3]School of Geography, Politics and Sociology, Newcastle University, Newcastle-upon-Tyne, United Kingdom
[4]School of Geography and Planning, University of Sheffield, Sheffield, United Kingdom

Key Points:

- Precipitation is the primary driver of wetland wetting and drying.
- Glaciers may attenuate the seasonal wetting and drying of nearby wetlands, but this effect reduces with downstream distance.
- Glacier retreat may increase the sensitivity of nearby wetlands to precipitation changes.

Corresponding author: R. Becker, r.becker@imperial.ac.uk

Abstract

High-altitude wetlands are critical ecosystems that store water, regulate downstream flows, and sustain biodiversity. Their persistence is tightly linked to continuous water inputs from precipitation, groundwater, snow and glacier melt, making them highly vulnerable to climate-driven shifts in mountain hydrology. Rapid glacier retreat, altered precipitation regimes, and rising temperatures are transforming water availability across mountain regions worldwide, but their consequences for wetland stability remain poorly understood. Here, using high-resolution satellite-based mapping (2019–2025) and statistical analyses, we investigate the spatiotemporal dynamics and hydroclimatic drivers of high-altitude wetlands at two tropical Andean study sites in Peru: Cordillera Vilcanota and La Raya. We demonstrate that precipitation is the primary driver of wetland seasonality, explaining up to 25% of the observed variability. This influence weakens in areas close to glaciers, where wetlands exhibit reduced seasonal fluctuations, suggesting a local dampening effect of glacial runoff on wetland wetting–drying cycles. Our spatially explicit analysis demonstrates that this dampening effect attenuates rapidly with distance and is no longer detectable beyond approx. 12 km from glaciers, indicating that the hydrological influence of glacier melt is highly localized and that most high-mountain wetlands are effectively decoupled from glacier-melt processes. The study highlights the critical role of glacier-wetland hydrological connectivity in the context of hydrological changes in mountain regions.

Plain Language Summary

High-altitude wetlands are important and unique ecosystems in mountain regions. They store water, support diverse plants and animals, and regulate water availability further downstream. These wetlands depend on a steady water supply, which makes them sensitive to climate change. In many mountain regions, glaciers are shrinking, rainfall patterns are shifting, and temperatures are rising. These changes affect the amount of water available throughout the year, but it remains unclear how mountain wetlands respond. In this study, we examine how wetlands have changed over time in two areas of the Peruvian Andes: one with glaciers and another where glaciers have recently disappeared. Using satellite images from 2019 to 2025, we track monthly changes in wetland extent and analyze how climate and water availability influence wetland behavior. We find that rainfall is the main factor controlling how wetlands expand or dry out. Wetlands near glaciers change less throughout the year, likely because glacier melt provides a more stable water source. This stabilizing

effect weakens rapidly with distance from glaciers and disappears beyond about 10 km, meaning most mountain wetlands are not influenced by glacier melt.

1 Introduction

Wetland ecosystems have long been recognized as vital for our global environment, due to their role as water and carbon stores, their importance as biodiversity hot-spots and their economic and cultural significance for local and indigenous communities (White-Nockleby et al., 2021). Ecologically, they provide nutritious forage for wild and domestic mammals, such as camelids (Cooper et al., 2019), purify water, decompose organic matter, and release nutrients into surface water (Salimi et al., 2021), thereby supporting biodiversity conservation (Mętrak et al., 2023). Hydrologically, they promote infiltration, recharge groundwater, and act as natural reservoirs by capturing excess seasonal runoff and gradually releasing it during subsequent dry periods, potentially buffering low flows and securing water availability (Barnett et al., 2005; Wu et al., 2025).

Due to their strong dependence on consistent and sufficient water inputs, wetlands are highly sensitive ecosystems. This vulnerability is especially pronounced in high mountain regions, where rapid glacier retreat and changing precipitation and temperature regimes are causing significant changes in mountain hydrology (Huss & Hock, 2018). With mountain glacier extent and volume projected to continue decreasing throughout the 21st century (Marzeion et al., 2020; Radić et al., 2014; Zekollari et al., 2025; Zemp et al., 2015), the nature and spatiotemporal patterns of glacier melt input will change, which may result in wetland degradation or loss and affect their ecosystem services (Haeberli & Weingartner, 2020). A key question, therefore, is the extent to which the dynamics of high-mountain wetlands in close proximity to glaciers are influenced by glacier meltwater contributions, and by glacier loss.

There is no universally accepted definition of high-mountain wetlands. Here, we define them as permanently or seasonally saturated areas located above the tree line and below the permanent snow line (Chatterjee et al., 2010). These wetlands typically develop in flat or gently sloping valley bottoms, over colluvial deposits and in infilled lakes (Emmer, 2024), where water can accumulate and create conditions that support year-round vegetation cover in otherwise harsh, rocky, and steep environments (Maldonado, 2014). Depending on their topographical position and proximity to glaciers and snowfields, high-mountain

wetlands may be sustained by varying contributions from precipitation, groundwater flow, snowmelt, and glacier runoff (Gribbin et al., 2024; Cooper et al., 2019; Ross et al., 2023), resulting in complex spatial patterns of their occurrences. The high variability in mountain temperature and precipitation further interacts with these fine-scale landscape features, producing highly heterogeneous environmental conditions that influence wetland persistence. Elevation, aspect, slope, and terrain complexity impact near-surface microclimates, leading to steep temperature gradients over short distances (Mountain Research Initiative EDW Working Group, 2015). Orographic uplift further enhances spatial precipitation variability, with windward slopes receiving substantially greater moisture inputs than leeward slopes (Rojas & Minder, 2024). Similarly, glacier melt processes depend on elevation, aspect, and slope, which generate strong spatial variation in melt rates and in the timing and magnitude of meltwater reaching downstream wetlands.

Due to this topographic and hydro-climatic complexity, the extent of hydrological connectivity between glaciers and mountain wetlands, and the subsequent impact of glaciological changes on wetlands is still unclear. While some studies have found no relationship between wetland and glacier melt dynamics (Cooper et al., 2019), others suggest that ongoing glacier retreat may initially drive wetland expansion, followed by a subsequent decline (Polk et al., 2017). Understanding hydrological connectivity between glaciers and wetlands is therefore key to assessing the impact of glacier retreat on mountain wetlands. Previous studies have addressed these questions using hydrogeological isotope analyses (Cooper et al., 2019; Gribbin et al., 2024) and local hydrological modeling studies (Ross et al., 2023). These methods require intensive data collection and data input, typically limiting their spatial coverage to single catchments and temporal resolution to short monitoring periods. Yet, due to the above mentioned topographic and hydro-climatic complexity in mountain regions, a longer-term and spatially explicit landscape-system perspective will enable the improved quantification of wetland–glacier connectivity and to predict how and most importantly, where ongoing hydro-climatic changes will alter wetland dynamics.

We hypothesize that wetlands located close to glaciers are hydrologically connected to glacier meltwater through surface and groundwater pathways, and that this connection influences inter- and intra-annual variability in wetland extent and moisture conditions. In such connected systems, reductions in glacier meltwater supply may therefore increase the risk of seasonal drying, although we do not expect complete wetland loss as precipitation reveals to remain a dominant driver, even near glaciers.

To test this hypothesis and to bridge the gap between local- and landscape system scale analyses, we use an unprecedented six-year time series of satellite-derived wetland observations to capture spatio-temporal wetland dynamics. We couple these observations with a spatially distributed regression analysis to identify the dominant drivers of wetland seasonality. Although this method does not allow direct identification of water source origins or subsurface flow pathways, it provides valuable insights into wetland behavior at landscape scale.

2 Methods and Data

2.1 Study sites

We focus our analysis on two high-altitude study sites in Southern Peru to test our hypothesis (Figure 1a-b). Both sites are experiencing rapid glacio-hydrological changes, driven by ongoing climate warming. While the Cordillera Vilcanota (Figure 1b, north) continues to host substantial glacier coverage (approx. 5.4% in our study site), the La Raya region (Figure 1b, south) has become largely ice-free in the past decades (glacier coverage $< 0.1\%$). The two study sites are located in close proximity to each other, in a semi-arid and High-Andean mountain landscape, around 3,300-6,000 m a.s.l.. Approximately 4-5% of both study sites are covered by wetlands, fed by rainfall, groundwater, and/or glacier melt. A strong precipitation seasonality, with a wet season from October to April and a dry season from May to September (Figure 1c-d) , drives a pronounced seasonal dynamic of wetlands extents (Gribbin et al., 2024; Ross et al., 2023).

The northern site encompasses a domain of 4,500 km^2 around the Cordillera Vilcanota (71°W, 13.7°S), the most extensive glacierized mountain range in the South of Peru and home to one of the world's largest tropical ice caps, the Quelccaya ice cap. Altitudes range from 3,260 to 6,030 m a.s.l.. Mean annual precipitation rates during our study period (2019-2025) are approx. 1420 mm/year. Mean monthly temperature variations are low and vary between 1.7°C and 4.5°C (Figure 1c), with colder temperatures during the dry season. Glaciers and the Quelccaya ice cap are rapidly shrinking (Taylor et al., 2022) and in the past six decades (1962-2020) the Cordillera Vilcanota has lost approx. 51% of its glacier coverage (INAIGEM, 2023b). The region's rapid glacier retreat makes it well suited for investigating meltwater effects on wetland dynamics and glacier-wetland hydrological connectivity.

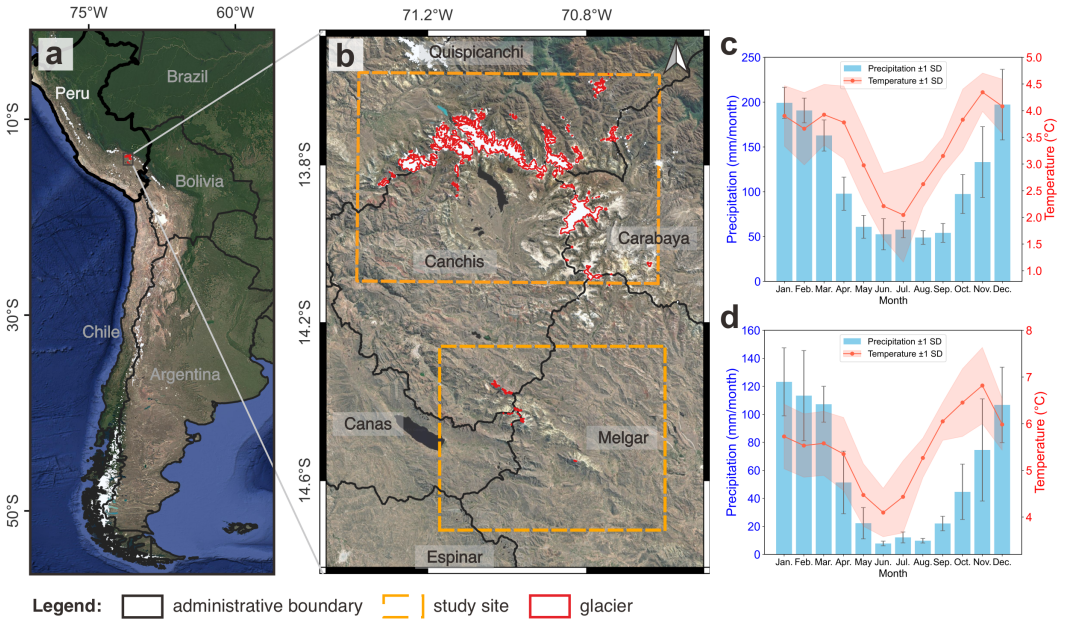

Figure 1. Location and climatic background of the two study sites. (a) Overview of the Andes and neighboring countries. (b) Enlarged view of the two study sites: the Cordillera Vilcanota in the north and La Raya in the south. Glacier outlines are from the Randolph Glacier Inventory (RGI) Version 7.0 (RGI Consortium, 2023), representing conditions around the year 2000. (c-d) Mean monthly precipitation and temperature from January 2019 to February 2025 (the study period) for the Cordillera Vilcanota (c) and La Raya (d). Precipitation was derived from the hourly IMERG product (Huffman et al., 2014), while temperature was obtained from the monthly averaged ERA5-Land dataset (Muñoz-Sabater et al., 2021).

Our southern study site is located approx. 60 km south of the Cordillera Vilcanota (71°W, 14.3°S) and spans a region of 3,100 km^2 around the La Raya mountain range, at altitudes between 3,880 to 5,270 m a.s.l.. This region has a more centered position on the Andean plateau and receives less precipitation than our northern site due to its larger distance and leeward position with respect to the prevailing advective moisture transport from the Amazon Basin (Drenkhan et al., 2015). Annual precipitation rates reach on average 713 mm/year. Mean monthly temperatures vary between 3.8°C and 6.9°C (Figure 1d). The Randolph Glacier Inventory, which has an approximate date of 2000, suggests the existence of small ice bodies at high elevations here (outlines shown in Figure 1b), but more contemporary satellite images show that the region has lost nearly the entirety of its glacier coverage, leaving many formerly ice-covered mountain tops and adjacent catchments

ice free. We selected this site to investigate wetland hydrology in a post-glacial landscape, where past hydrological connectivity between glaciers and wetlands may have existed but has been disconnected by continued glacier retreat.

2.2 Quantifying temporal and spatial wetland extents

We mapped wetlands and their temporal dynamics using monthly satellite imagery from January 2019 to February 2025, building on the approach of Ross et al. (2023). Spectral, topographic, and ecological data were compiled from Sentinel-1 and Sentinel-2 imagery, the 30-m NASA SRTM DEM, and the RESOLVE ecoregions (Dinerstein et al., 2017). Within defined training areas, we extracted random samples to derive predictor variables including surface-moisture indices, vegetation indices, as well as topographic and ecological metrics (Figure S1 and Text S1 in Supporting Information S1). These predictors informed a Random Forest classifier, which we used to map high-altitude wetlands. With this approach we achieved an average mapping accuracy of 91% (± 1%) when validated against an existing wetland dataset (INAIGEM, 2023a). Monthly wetland extents were generated by repeating the classification for monthly image subsets. To address data gaps from cloud cover in the wet season, we applied a 3-month rolling window, to build 3-monthly image composites and assigned the resulting average extent to the central month. To analyze spatial patterns in wetland dynamics, we delineated sub-catchments from the SRTM DEM using a 5,000-pixel contributing-area threshold and quantified monthly wetland area within each unit (See Supporting Information S1 and S2 for details on the mapping approach and thresholding).

2.3 Gridded precipitation and temperature data

Monthly precipitation data were obtained from the hourly IMERG product, a satellite-based precipitation estimate from NASA's GPM mission (Huffman et al., 2014), with a spatial resolution of 0.1° x 0.1°. For the regression analysis, monthly precipitation totals were extracted at the centroid of each sub-catchment, to match the spatial unit of the wetland analysis. Temperature data was obtained from the monthly averaged ERA5-Land dataset (Muñoz-Sabater et al., 2021), at a resolution of 0.1° x 0.1°. Similarly to the precipitation data extraction, we extracted the mean monthly temperature value for each sub-catchment at its respective centroid, to account for spatial temperature variations.

2.4 Glacier-dilution algorithm and distance group classification

In the absence of spatially distributed observations of glacier meltwater, we developed an algorithm to approximate the downstream attenuation of meltwater influence within the river network. Based on the Strahler stream order (Strahler, 1957) and flow accumulation, we ranked single stream segments of the river network. Glacier-proximal segments were assigned a maximum meltwater signal. This signal was progressively diluted at each stream confluence as non–glacier-fed tributaries entered the network, producing a continuous index of relative glacier influence for each stream segment (see detailed methodology in Text S3 and Figure S4 in Supporting Information S3). Each sub-catchment was then assigned the index of its longest intersecting stream segment. Subsequently, the sub-catchments were grouped into the three classes "close", "medium", and "far", indicating not only the distance to glaciers but also the potential glacier melt influence in each of the sub-catchment's main stream. The glacial impact propagation maps and the distributions of glacial impact categories for the two study sites are presented in Figure 2.

In the glacierized Cordillera Vilcanota, the three categories "close", "medium", and "far" from glaciers and glacial impact, reflect present-day conditions as glaciers are still present and abundant. In La Raya, where current glacier extent is minimal, the same classification was applied using the glacier outlines from the year 2000 (Pfeffer et al., 2014). Here, the three categories refer to potential former distances and strengths of glacier melt impacts. Using the same classification approach in both regions allows a direct comparison of wetland dynamics across equivalent distance–influenced classes. This enables us to distinguish effects attributable to glacier meltwater from those arising from other factors such as topography or climatic drivers. Although hydrological connectivity between glacier-fed streams and wetlands are still debated and wetlands may be decoupled from streamflow (Gribbin et al., 2024; Cooper et al., 2019), our approach still provides a useful proxy for relative meltwater influence. By following the stream network, the glacier melt influence does not rely on distance alone, but it implicitly incorporates the effects of topography and drainage pathways. This makes it a more hydrologically informed indicator of potential meltwater contributions than a simple distance-based metric.

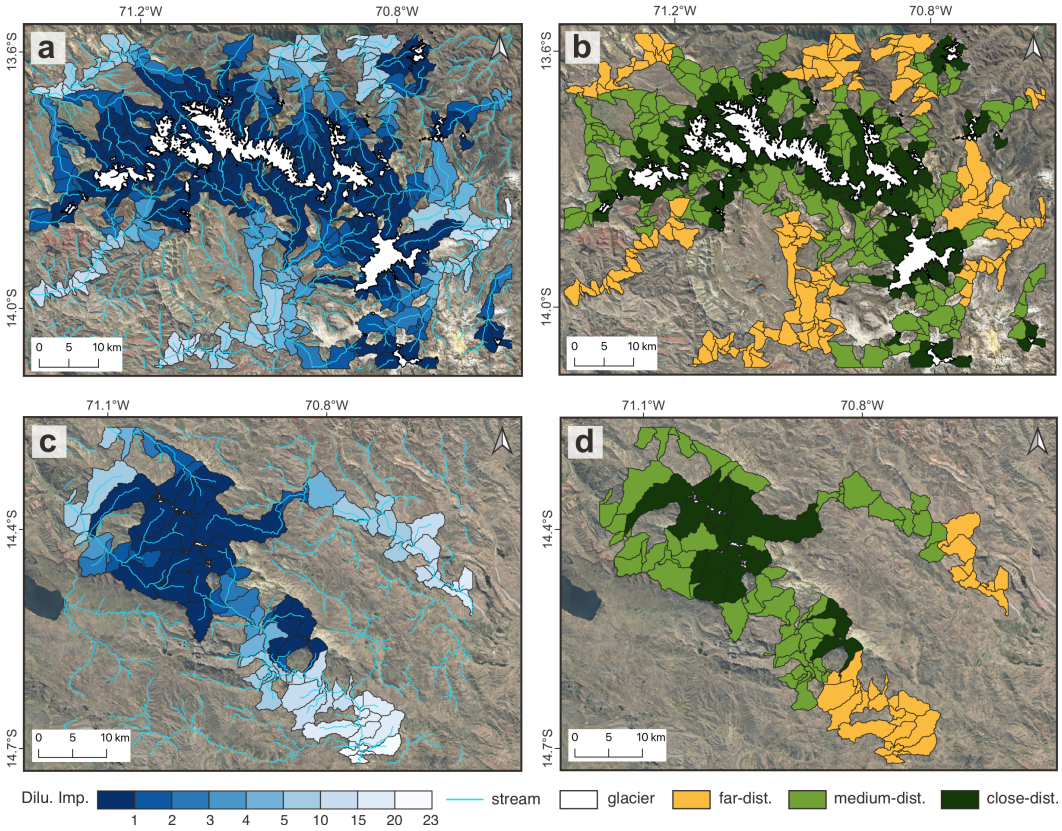

Figure 2. Glacial impact propagation maps and the associated three distance groups in the Cordillera Vilcanota (a-b) and the La Raya (c-d): glacier dilution with stream networks (a, c) and distance groups (b,d).

2.5 Multiple linear regression analysis

Multiple linear regression analysis was applied to identify the main hydro-climatic drivers (predictor variables) of wetland dynamics (response variable) and to quantify their independent contributions. Predictor variables included monthly average temperature and precipitation, as well as seasonality and long-term trends. The general form of the regression equation is given below:

$$\tilde{Y} = \alpha_0 + \sum_{i=1}^{n} \alpha_i \tilde{X}_i \tag{1}$$

All variables (Y and X_i) were standardized prior to regression as $\tilde{Z} = (Z - \bar{Z})/\sigma_Z$, where Z represents either Y or any X_i; $\bar{Z}$ is the mean of the original variable Z; and σ_Z is its standard-deviation (SD). $\tilde{Y}$ is then the standardized dependent variable; $\tilde{X}_i$ is the standardize predictor for sub-catchment i; and α_i is its regression coefficient.

To explicitly account for the strong seasonal cycle, we included seasonality indicators as predictor variables to improve our model accuracy by isolating recurring seasonal patterns. For this, each month was mapped onto a unit circle, and the sine and cosine of the month were used as predictors instead of raw numerical values (January=1, ..., December=12), thereby avoiding undue emphasis on December and ensuring a continuous representation of seasonality. For subsequent analyses, the amplitude of the seasonal cycle (S) was derived from the sine and cosine components as

$$S = \sqrt{\alpha_{\sin}^2 + \alpha_{\cos}^2} \tag{2}$$

which represents the combined magnitude (Euclidean length) of the standardized regression coefficients $\alpha_{\sin}$ and $\alpha_{\cos}$. The trend indicator is defined as a time-ascending index, ranging from 1 (as January 2019) to 74 (as February 2025).

As several predictors exhibit strong intercorrelations, Ridge regression was applied to mitigate the effects of multicollinearity. Ridge regression introduces an L2 regularization term to the loss function, penalizing large coefficient values and allowing correlated predictors to share explanatory power more evenly (McDonald, 2009). The Ridge estimator $\widehat{\alpha}$ is obtained by minimizing the residual sum of squares (RSS) plus an L2 penalty term (Marquardt & Snee, 1975), as expressed in Eq. 3. The optimal set of coefficients was selected by cross-validation (80% training, 20% testing) based on achieving a higher determination coefficient ($R^2 > 0.7$) and a lower normalized root-mean-square error (NRMSE < 0.2).

$$\widehat{\alpha} = \arg\min_{\alpha} \Big\{ \underbrace{\sum_{i=1}^{n} (y_i - \mathbf{x_i^T}\alpha)^2}_{\text{RSS}} + \underbrace{\lambda \sum_{j=1}^{p} a_j^2}_{\text{L2 penalty term}} \Big\} \tag{3}$$

In Eq. 3, $\widehat{\alpha}$ denotes the estimated coefficient vector under the Ridge penalty, where $\alpha = (\alpha_1, \ldots, \alpha_p)^{\mathsf{T}}$ represents the regression coefficients to be estimated. y_i is the response variable for sub-catchment i, $\mathbf{x}_i = (x_{i1}, \ldots, x_{ip})^{\mathsf{T}}$ is the predictor vector for sub-catchment i, n is the number of sub-catchments, p is the number of predictors, and $\lambda \geq 0$ is the regularization parameter. As λ increases, the coefficients are increasingly shrunk toward zero.

Predictors ($\tilde{X}_i$) and the response variable ($\tilde{Y}$) were standardized using statistics derived from the full study-area dataset rather than from individual sub-catchments, to assess the relative strength of each variable and enable comparisons across sub-catchments. Accordingly, a coefficient of 1 represents that a 1–SD increase in the predictor corresponds to a 1–SD increase in the response. Larger coefficients therefore reflect stronger effects, allowing

the importance of predictors to be directly ranked and compared by coefficient magnitude. Table 1 summarizes the physical meaning of one SD for each predictor and for the wetland response variable in both study sites.

Table 1. Physical meaning of one SD for each predictor, including temperature (tempr.), precipitation (precip.), seasonality (seasonal.), and trend, and for the response variable (wetland).

Study site	predictors				
	tempr. (°C)	*precip.* (mm)	*seasonal.* (-)	*trend* (months)	*wetland* (km^2)
Cord. Vilcanota	1.92	76.58	0.71	21.36	0.35
La Raya	1.57	42.68	0.71	21.36	0.84

We applied a cross-Spearman correlation analysis to identify the most significant time lag between the wetland series and the climatic predictors (Text S4 in Supporting Information S4). This analysis showed that a 3-month lag resulted in the strongest and most significant relationship in the Cordillera Vilcanota region. For consistency and direct comparison, we adopted the same lag for the southern site. Based on these correlation results, we applied 3-month time lag to temperature and precipitation in all regression models to best capture the wetland response to climatic variability. Separate regression models were constructed for each sub-catchment at the two study sites to assess the spatially distributed effects of climatic drivers on wetland dynamics and to evaluate how glacial presence modulates these effects. We then performed 500 bootstrap resampling iterations to assess the robustness of each regression coefficient. Only statistically significant values were retained. For each distance group, the mean, standard error, and corresponding 95 % confidence intervals of these significant coefficient samples were then calculated based on the Student's t-distribution.

3 Results and Discussion

3.1 Seasonality of wetlands

In both study regions, wetlands show pronounced temporal variability that reflects the strong seasonality of precipitation. Wetland extent expands during the wet season and contracts during the dry season, with a characteristic three-month lag between peak rainfall

and maximum wetland extent (Figure 3a, c). This delay likely reflects two hydrological and ecological processes: (i) the time required for rainfall to infiltrate, recharge groundwater, and subsequently supply wetlands through hillslope discharge (Cooper et al., 2019; Gribbin et al., 2024; Ross et al., 2023); and (ii) the delayed onset of vegetation greening following the start of the rainy season, which is captured by our remote-sensing–based wetland detection that is particularly sensitive to photosynthetically active, green surface features (Dangles et al., 2017). Across all three glacier–distance classes (close, medium, far), wetlands show the same precipitation response time, reinforcing the conclusion that precipitation is the dominant driver of seasonal wetland dynamics, even in glacier–proximal areas.

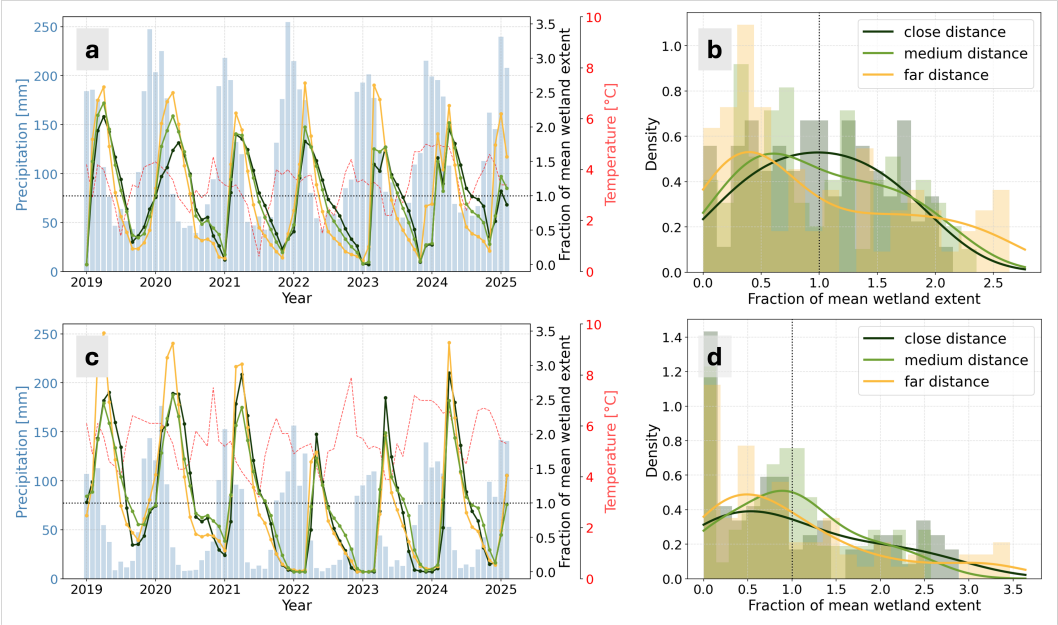

Figure 3. Seasonal wetland dynamics around the Cordillera Vilcanota (a, b) and around the La Raya mountains (c, d) in close, medium and far distances from (formerly) glacierized areas. We show the fraction of mean wetland extents instead of the total wetland extents, to allow a comparison between our three distance classes.

Despite this strong precipitation-driven pattern, clear spatial differences can be observed. In the still-glacierized Cordillera Vilcanota region, sub-catchments close to glaciers display a reduced seasonal amplitude in wetland extent (Figure 3a) and a unimodal distribution (Figure 3b), indicating more stable year-round wet conditions. In contrast, sub-catchments far from glaciers show the largest seasonal wetland fluctuations and a distinct bimodal distribution, reflecting pronounced wetting and drying cycles. Wetlands at inter-

mediate distances exhibit transitional behavior. These patterns suggest that glacier meltwater exerts a buffering effect on wetland variability, stabilizing wetland extents in glacier-proximal areas. This effect however diminishes rapidly and is no longer detectable in the far-distance class.

In the La Raya region, where current glacier meltwater inputs are minimal or absent, wetland dynamics do not differ between sub-catchments close to or far from formerly glaciated areas (Figure 3c, d). Inter-annual variability in wetland extent is substantially larger than in the Cordillera Vilcanota region (CV = 0.75 vs. 0.54), and wetlands frequently dry out during the dry season (e.g., in 2022–2024). These observations point to a strong dependency on seasonal precipitation and the absence of a stabilizing influence from glacier meltwater.

3.2 Hydro-climatic drivers of wetland dynamics

3.2.1 Precipitation

The results from our regression analysis confirm that precipitation is the dominant driver of wetland extent in both study sites. Precipitation lagged by three months, explains approx. 19–21 % and 18–25 % of wetland variability in the Cordillera Vilcanota and La Raya mountain ranges, respectively (Table 2, see detailed calculation in Text S6 in Supporting Information S6).

Table 2. The average explained variance (%) and its corresponding 95 % confident intervals (CI) across distance groups at two study sites.

Study site	Distance to glaciers	Variables			
		temperature	*precipitation*	*seasonality*	*trend*
Cordillera Vilcanota	far dist.	1.7 ± 5.7	20.9 ± 1.8	32.4 ± 2.2	6.3 ± 1.0
	medium dist.	4.3 ± 1.5	20.1 ± 1.3	31.0 ± 1.4	6.3 ± 0.6
	close dist.	3.5 ± 2.3	19.0 ± 2.2	31.8 ± 2.6	7.2 ± 1.8
La Raya	far dist.	/	25.0 ± 3.7	17.0 ± 2.3	5.6 ± 0.6
	medium dist.	/	18.2 ± 1.4	26.7 ± 3.5	5.5 ± 0.7
	close dist.	/	20.7 ± 2.5	29.3 ± 3.8	5.0 ± 1.6

In the glaciated Cordillera Vilcanota region, precipitation plays a stronger role in sub-catchments located farther from glaciers (yellow lines), which also tend to exhibit higher seasonal variations (Figure 4a), underlining our results presented above. Wetland sensitivity to precipitation increases with distance from glaciers, with average coefficients rising from 0.14 ($\pm$ 0.05) in glacier-proximal areas to 0.26 ($\pm$ 0.09) farther away (Figure 5a). In the southern and northwestern parts of the region, precipitation coefficients commonly exceed 0.5, and in some cases 2.0, indicating particularly strong precipitation control. Some regions in the northeastern and southwestern parts of this study site do not follow this pattern, but here precipitation–wetland relationships are statistically insignificant and therefore less reliable. A 1–SD increase in precipitation ($\approx$ 76.6 mm per month; Table 1) expands wetland extent by up to 0.12 km^2 in distant sub-catchments, which corresponds to roughly four times the response observed in glacier–proximal ones. Similarly, a 1–SD (0.71; Table 1) increase

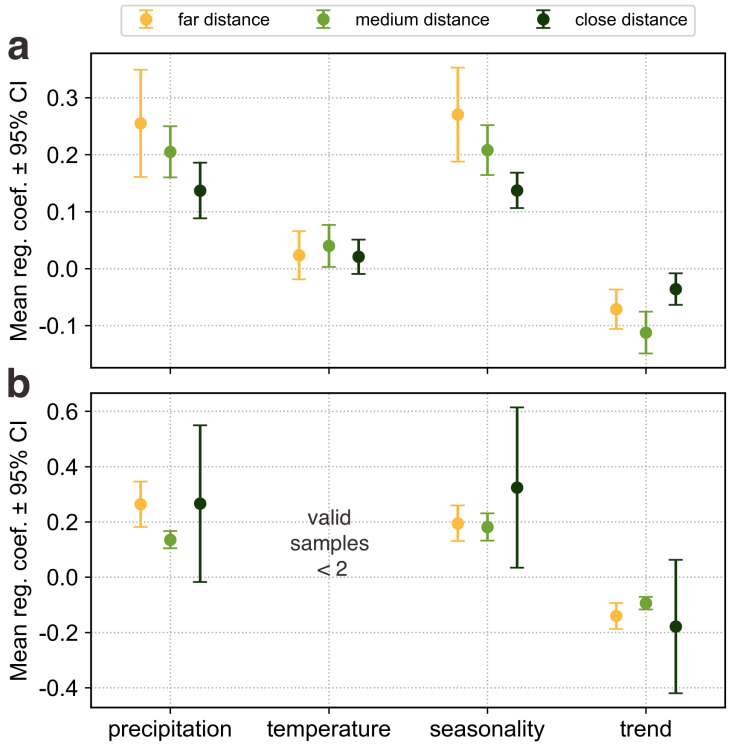

Figure 4. The average value of significant regression coefficients (reg. coef.) and its related 95 % confidence interval (CI) across the three distance classes in the Cordillera vilcanota (a) and in the La Raya (b). Precipitation, temperature, and trend were predictive variables in the Ridge regression, while seasonality was derived from $\alpha_{\sin}$ and $\alpha_{\cos}$. The detailed values were shown in Table S1 in Supporting Information S5.

in seasonality corresponds to an expansion of approximately 0.12 km^2 in the more distant sub-catchments, but only about 0.04 km^2 in glacier–proximal ones. This indicates that wetlands distant from glacier influence are roughly three times more sensitive to seasonal variability than those nearby.

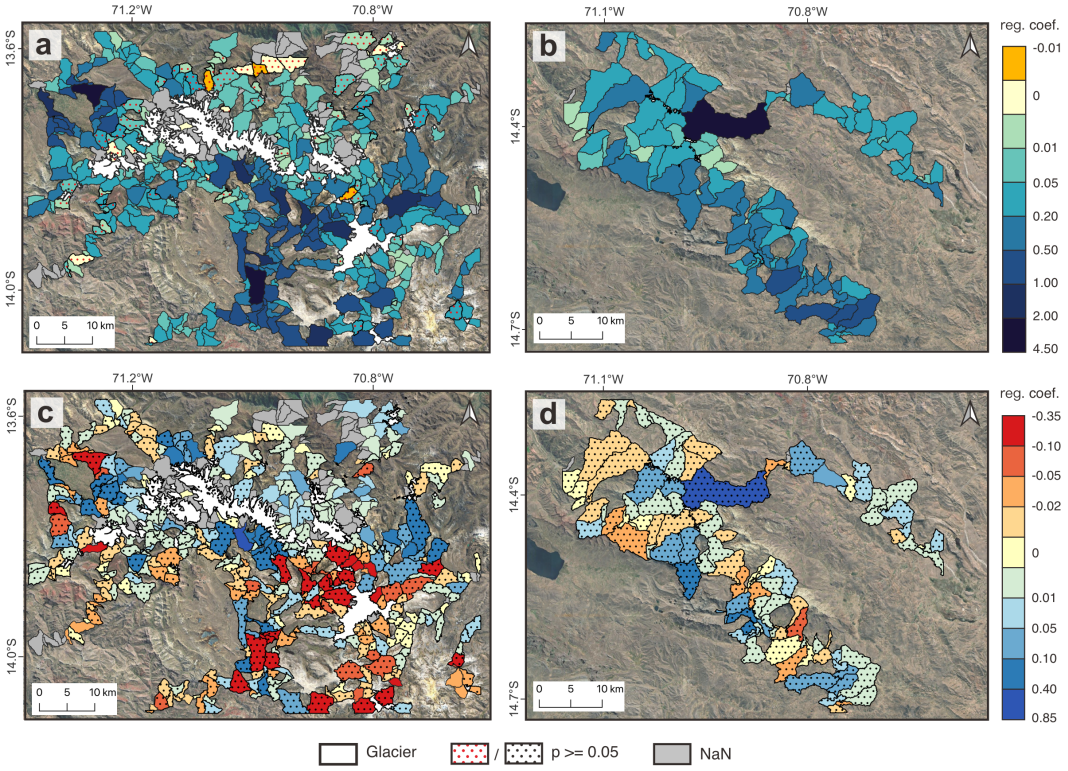

Figure 5. Ridge regression coefficients for precipitation (a-b) and temperature (c-d) across three distance classes in each sub-catchment at both study sites: (a, c) the Cordillera Vilcanota; (b, d) the La Raya region.

In the La Raya region, these distinct spatial variations in precipitation influence and seasonality across the distance groups are not apparent (Figure 4b) and the effect of precipitation becomes more spatially heterogeneous (Figure 5b). No clear distinction is observed between the far- and close-distance classes, both showing average coefficients of around 0.26. Within the close-distance group, the effects of precipitation and seasonality become markedly less stable, with the 95% confidence interval expanding by a factor of six for precipitation and ten for seasonality. Although average precipitation coefficients in the far-distance groups are similar between regions ($\approx$ 0.26), the corresponding wetland response differs. In the La Raya region, a 1–SD increase in precipitation ($\approx$ 42.7 mm per month;

Table 1)—about 56% of the SD in the Cordillera Vilcanota—results in 2.4 times greater wetland expansion. This indicates a proportionally stronger dependence on precipitation in the deglaciated La Raya landscape. These patterns align with our earlier findings, indicating once more that precipitation dominates wetland expansion and shrinkage.

The spatially distributed results at sub-catchment level (Figure 5a, b) further indicate that both rainfall amount and overall sub-catchment wetland extent (Figure S5 in Supporting Information S7) modulate wetland sensitivity to precipitation variability. In the north-eastern Cordillera Vilcanota region, located on the windward slope facing the Amazon basin, mean precipitation is higher but the relationship between rainfall and wetland dynamics is weak or statistically insignificant. In contrast, in the drier La Raya mountain range, wetlands show a stronger precipitation dependency and a more pronounced intra- and inter-annual variability.

Overall, the strong control of precipitation on wetland dynamics is consistent with previous research, which shows that high-Andean wetlands are primarily sustained by direct precipitation and hillslope groundwater discharge recharged by rainfall (Gribbin et al., 2024; Cooper et al., 2019; de la Fuente et al., 2021). Isotope evidence from Cooper et al. (2019) shows that wetland hydrology in the high central Andes remains largely independent of glacier runoff, with meltwater bypassing wetlands via stream channels. This assumption, that wetland and glacier dynamics represent two separate systems, would explain the strong seasonal drying and wetting of wetlands in response to rainfall, even in sub-catchments with potentially high glacier melt contribution. It also explains the persistence of wetlands and their maintained seasonality in the La Raya mountain region, where glaciers have already disappeared in most sub-catchments, and where precipitation is the only remaining water source (Figure 3c).

3.2.2 Temperature

Temperature effects are generally weak across both study sites (Figure 5c, d). Most sub-catchments show statistically insignificant relationships with temperature, and no distance-dependent pattern emerges. Temperature coefficients are consistently smaller than precipitation coefficients. A 1–SD increase in temperature in the Cordillera Vilcanota (corresponding to around 2 °C; Table 1) results in a standardized wetland response ranging from -0.01 to

0.07 SD (from -0.008 km^2 to +0.06 km^2). The effect of temperature in the La Raya is generally statistically insignificant.

In the Cordillera Vilcanota, average coefficients are similar across distance groups (0.03 $\pm$ 0.04), yet individual sub-catchments display contrasting responses. Some glacier–proximal sub-catchments show negative coefficients (< -0.1), suggesting drying with higher temperatures, while others exhibit positive coefficients (> 0.1), indicating a wetting effect (Figure 5c). Similar inconsistencies also occur in sub-catchments farther from glaciers and within the La Raya region (Figure 5d). These opposing local responses, combined with predominantly insignificant coefficients, suggest that temperature effects are highly variable and should be interpreted with caution.

Overall, these results are contrary to our expectations. A stronger positive temperature–wetland relationship might be expected in glacier–proximal areas of the Cordillera Vilcanota if warmer periods enhanced meltwater inputs. The absence of such a pattern suggests that the relatively small seasonal temperature range (1.7–4.5 °C) does not substantially increase glacier meltwater contributions. This is also confirmed by Fyffe et al. (2021), who found that rather than temperatures, intense radiative fluxes and their surface albedo are the primary drivers of glacier melt in this region, which can result in ablation in low temperatures. In the La Raya mountains, where glacier cover is minimal (0.1%) and temperature variability is similarly limited (3.8–6.9 °C), temperature changes and glacier areas are likely insufficient to generate additional meltwater to influence wetland extents.

The limited role of temperature may also partly reflect the nature of our regression approach, which attributes most of the explained variability to the dominant precipitation signal. This does not imply that temperature effects are absent. Rather, their relative contribution is small and therefore masked by stronger precipitation-driven dynamics. Furthermore, we only consider monthly temperature variations, in a region where daily temperature and radiation fluctuations are high and can cause significant variations in glacier melt runoff. In addition, the chosen 6-year time period is too short to show any long-term temperature trends, which could impact long-term wetland dynamics.

3.2.3 Glacier melt

While our analysis does not allow direct quantification of glacier melt contributions, several independent results support our hypothesis, that wetlands located close to glaciers are

hydrologically connected to glacier melt. A key result is the decline in the regression coefficients of precipitation and seasonality towards glacier–proximal areas (precipitation: 0.26 → 0.14; seasonality: 0.27 → 0.14; Figure 4a). This reduced precipitation importance indicates that additional water sources, such as glacier melt, gain influence near glaciers and help buffer seasonal wetland variations. This interpretation aligns with isotope evidence from Gribbin et al. (2024), who detected a small but measurable glacier-melt contribution to wetland waters in a glaciated catchment in the Cordillera Vilcanota region. The buffering effect however is highly localized and detectable within approx. 2.8 km of glacier margins, already weakened by approx. 5 km, and dominated by precipitation beyond approx. 12 km (Table 3). This aligns with the observation that wetland extents show a unimodal distribution in close proximity to glaciers, indicating higher wetland stability, while wetlands in farther distance to glaciers and in our deglaciated site, indicate a clear bi-modal wetting-drying seasonality (Figure 3b, c). Consistent with previous work (Buytaert et al., 2017), glacier-melt impacts thus diminish rapidly downstream. The absence of this distance-dependent pattern in the largely deglaciated La Raya region (Figure 4b) further supports our hypothesis. Here, wetland dynamics are even stronger driven by precipitation (average coefficient 0.27 ± 0.30 vs. 0.14 ± 0.05 in the Cordillera Vilcanota), reflected in faster dry-season wetland contraction and occasional full desiccation (Figure 3c).

Table 3. Summary of sub-catchment distances to the 2000 glacier outlines across distance groups using trimmed means and 5th–95th percentile statistics in both study sites.

	Cordillera Vilcanota			La Raya		
	p5 (km)	mean (km)	p95 (km)	p5 (km)	mean (km)	p95 (km)
close dist.	1.3	2.8	4.9	2.8	6.0	12.3
medium dist.	2.0	5.0	10.3	3.6	10.0	22.1
far dist.	5.6	11.7	21.6	7.9	17.9	25.7

Hence, our spatially resolved analysis reveals systematic distance-related patterns that refine the previously stated assumption, that wetlands and glaciers represent two separate hydrological systems. We argue that although glacier-fed streams and wetlands may appear disconnected when examined at broader catchment extents, localized hydrological linkages still occur in glacier–proximal environments. The apparent discrepancy with earlier studies

(Cooper et al., 2019) likely reflects scale effects. While glacier melt may influence wetlands at very short distances, this signal diminishes rapidly along the drainage network and becomes undetectable even at modestly larger spatial scales.

We note that our interpretation of spatial patterns in wetland dynamics relies on glacier proximity and stream networks, but does not fully account for the complex geomorphological context of high mountain wetlands. Wetlands in high mountain regions are located in very complex geomorphological environments that include a variety of glacial and Quaternary landforms, such as moraines, glacial lakes, kettle lakes, and tallus or debris deposits (Glas et al., 2018; Chesnokova et al., 2020). These landforms often host aquifers of high permeability and storage capacities (Emmer, 2024; Ó Dochartaigh et al., 2019), which might contribute to the buffered seasonality as additional water stores. Our remote-sensing–based approach cannot separate their contribution from glacier melt effects. However, the fact that the buffering signal is only observed in the glacierized Cordillera Vilcanota study site suggests that these stores might be at least partly glacier-fed. In the La Raya mountain range similar peri-glacial landforms and hence, potential alternative water stores exist, but they do not exhibit the same buffering effect.

In conclusion, our spatially distributed analysis shows that glacier melt contributes measurably to wetland hydrology, but that this influence remains localized and does not extend beyond a few kilometers from glacier margins ($\approx$ 1–5 km in the Cordillera Vilcanota). Beyond this distance, precipitation and likely precipitation-recharged groundwater dominate wetland variability, consistent across both glacierized and deglaciated catchments. The rapid downstream attenuation of glacier influence explains why glacier–wetland linkages are not detected at broader catchment scales. The strong precipitation dominance makes wetlands more susceptible to pronounced intra- and interannual fluctuations, leading to higher annual wetting–drying amplitudes in disconnected glacier–wetland systems (Figure 6).

3.3 Limitations and uncertainties

The regression analysis considers a constant 3-month time lag between wetland dynamics and environment drivers for all sub-catchments. While this time lag correctly reflects the catchment-scale and distance-class response, wetland response to precipitation and temperature may vary between sub-catchments depending on topography and runoff pathways. Furthermore, snow processes are simplified in our analysis. While snow is included in total

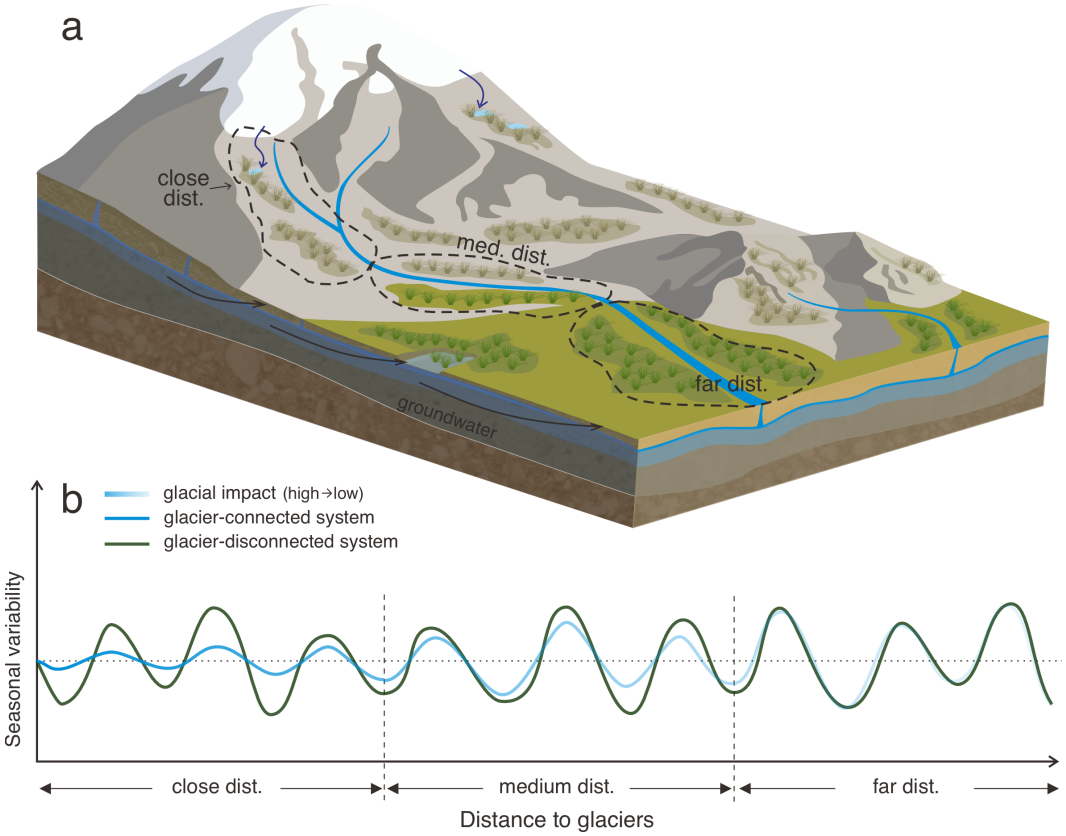

Figure 6. Conceptual model of high-Andean wetlands across the three distance classes (a) and the seasonality variability in glacier-connected and -disconnected wetland systems (b).

precipitation, we do not explicitly separate snowmelt from rainfall or account for melt timing. In our high Andean sites, rapid melt, limited snow pack and the prevalence of sublimation justify this assumption (Fyffe et al., 2021), though short-term meltwater contributions may be underestimated. In addition to climatic controls, human management practices such as irrigation can substantially alter high-Andean wetland dynamics. In the Peruvian Andes, irrigation of wetlands allows some wetlands to remain green during the dry season (Verzijl & Quispe, 2013; Monge-Salazar et al., 2022; Buytaert et al., 2006), leading our satellite-based approach to classify them as permanently wet despite underlying seasonality. This can bias estimates of wetting–drying cycles and the inferred role of glacier melt. Hence, part of the observed dampened wetland variability may reflect human intervention rather than natural hydro-climatic drivers. Finally, our assessment is based on only two study areas. Although these two sites contrast clearly the difference between wetlands in glaciated and deglaciated landscapes, regional variability may exist. Broader analyses at larger scale but at high

spatial resolution are therefore needed to capture the full range of Andean glacier-wetland connectivity.

4 Conclusions

Using six years of high-resolution wetland maps and spatially distributed regression analysis, we demonstrate how glacier–wetland connectivity shapes high-Andean wetland dynamics in southern Peru. Although precipitation dominates wetland variability in our glacierized as well as in our largely deglaciated study sites, a strong spatial gradient emerges in areas that receive meltwater inputs. Wetlands situated in close proximity to glacier margins show a reduced seasonality, indicating persistent water availability throughout the year. This pattern suggests that glacier meltwater is dampening the magnitude of wetting–drying cycles that would otherwise be driven by precipitation alone. Sub-catchments that lose direct glacier–wetland connectivity rely increasingly on rainfall, resulting in more pronounced seasonality and greater sensitivity to dry-season moisture deficits. This rapid spatial transition from meltwater-buffered to precipitation-dominated wetlands reveals that glacier–wetland linkages are limited to a relatively narrow upstream zone. Ongoing glacier retreat will therefore most likely have only very localized impacts on wetlands.

Methodologically, our remote-sensing and regression framework provides a scalable approach to resolve spatial heterogeneity in wetland–glacier and wetland–climate linkages, even though it cannot directly distinguish individual water sources or subsurface pathways. By revealing systematic distance-dependent gradients in glacier influence, our study shows how such a spatially explicit landscape–system approach can help to assess highly localized wetland–glacier connectivity.

Author Contribution

D. Xuan and R. Becker designed the research and contributed equally to this work.

Conflict of Interest

The authors declare there are no conflicts of interest for this manuscript.

Data Availability Statement

Data and analysis code will be made publicly available upon publication.

Acknowledgments

This work was supported by the Natural Environment Research Council highlight topic grant Deplete and Retreat (NE/X004031/1), to J. C. Ely, W. Buytaert and B. Davies, and which supported R. Becker and O. King.

References

Barnett, T. P., Adam, J. C., & Lettenmaier, D. P. (2005). Potential impacts of a warming climate on water availability in snow-dominated regions. *Nature*, *438*(7066), 303–309.

Buytaert, W., Célleri, R., De Bièvre, B., Cisneros, F., Wyseure, G., Deckers, J., & Hofstede, R. (2006). Human impact on the hydrology of the andean páramos. *Earth-Science Reviews*, *79*(1-2), 53–72.

Buytaert, W., Moulds, S., Acosta, L., De Bièvre, B., Olmos, C., Villacis, M., … Verbist, K. M. (2017). Glacial melt content of water use in the tropical andes. *Environmental Research Letters*, *12*(11), 114014.

Chatterjee, A., Blom, E., Gujja, B., Jacimovic, R., Beevers, L., O'Keeffe, J., … Biggs, T. (2010). Wwf initiatives to study the impact of climate change on himalayan high-altitude wetlands (haws). *Mountain Research and Development*, *30*(1), 42–52.

Chesnokova, A., Baraër, M., Laperrière-Robillard, T., & Huh, K. (2020). Linking mountain glacier retreat and hydrological changes in southwestern yukon. *Water Resources Research*, *56*(1), e2019WR025706.

Cooper, D. J., Sueltenfuss, J., Oyague, E., Yager, K., Slayback, D., Caballero, E. M. C., … Mark, B. G. (2019). Drivers of peatland water table dynamics in the central andes, bolivia and peru. *Hydrological Processes*, *33*(13), 1913–1925.

Dangles, O., Rabatel, A., Kraemer, M., Zeballos, G., Soruco, A., Jacobsen, D., & Anthelme, F. (2017). Ecosystem sentinels for climate change? evidence of wetland cover changes over the last 30 years in the tropical andes. *PloS one*, *12*(5), e0175814.

de la Fuente, A., Meruane, C., & Suárez, F. (2021). Long-term spatiotemporal variability in high andean wetlands in northern chile. *Science of the Total Environment*, *756*, 143830.

Dinerstein, E., Olson, D., Joshi, A., Vynne, C., Burgess, N. D., Wikramanayake, E., … others (2017). An ecoregion-based approach to protecting half the terrestrial realm. *BioScience*, *67*(6), 534–545.

Drenkhan, F., Carey, M., Huggel, C., Seidel, J., & Oré, M. T. (2015). The changing water cycle: climatic and socioeconomic drivers of water-related changes in the andes of peru.

Wiley Interdisciplinary Reviews: Water, *2*(6), 715–733.

Emmer, A. (2024). Infilled lakes (p ampas) of the cordillera blanca, peru: Inventory, sediment storage, and paleo outbursts. *Progress in Physical Geography: Earth and Environment*, *48*(2), 208–230.

Fyffe, C. L., Potter, E., Fugger, S., Orr, A., Fatichi, S., Loarte, E., … others (2021). The energy and mass balance of peruvian glaciers. *Journal of Geophysical Research: Atmospheres*, *126*(23), e2021JD034911.

Glas, R., Lautz, L., McKenzie, J., Mark, B., Baraer, M., Chavez, D., & Maharaj, L. (2018). A review of the current state of knowledge of proglacial hydrogeology in the cordillera blanca, peru. *Wiley Interdisciplinary Reviews: Water*, *5*(5), e1299.

Gribbin, T., Mackay, J. D., MacDonald, A., Hannah, D. M., Buytaert, W., Baiker, J. R., … others (2024). Bofedal wetland and glacial melt contributions to dry season streamflow in a high-andean headwater watershed. *Hydrological Processes*, *38*(8), e15237.

Haeberli, W., & Weingartner, R. (2020). In full transition: Key impacts of vanishing mountain ice on water-security at local to global scales. *Water Security*, *11*, 100074.

Huffman, G. J., Bolvin, D. T., Braithwaite, D., Hsu, K., Joyce, R., & Xie, P. (2014). Integrated multi-satellite retrievals for gpm (imerg). *Precipitation Measurement Missions Technical documentation.*

Huss, M., & Hock, R. (2018). Global-scale hydrological response to future glacier mass loss. *Nature Climate Change*, *8*(2), 135–140.

INAIGEM. (2023a). *Memoria descriptiva del inventario nacional de bofedales del perú 2023* (Tech. Rep.). Huaraz, Perú: Instituto Nacional de Investigación en Glaciares y Ecosistemas de Montaña.

INAIGEM. (2023b). *Memoria descriptiva del inventario nacional de glaciares y lagunas de origen glaciar del perú* (Tech. Rep.). Huaraz, Perú: Dirección de Investigación en Glaciares (DIG) - Instituto Nacional de Investigación en Glaciares y Ecosistemas de Montaña (INAIGEM).

Maldonado, M. (2014). An introduction to the bofedales of the peruvian high andes. *Mires and Peat*, *15*(5), 1–13.

Marquardt, D. W., & Snee, R. D. (1975). Ridge regression in practice. *The American Statistician*, *29*(1), 3–20.

Marzeion, B., Hock, R., Anderson, B., Bliss, A., Champollion, N., Fujita, K., … others (2020). *Partitioning the uncertainty of ensemble projections of global glacier mass change,*

earth's future, 8, e2019ef001470.

McDonald, G. C. (2009). Ridge regression. *Wiley Interdisciplinary Reviews: Computational Statistics*, *1*(1), 93–100.

Mętrak, M., Chachulski, Ł., Pawlikowski, P., Rojan, E., Sulwiński, M., & Suska-Malawska, M. (2023). Potential role of high-altitude wetlands in preservation of plant biodiversity under changing climatic conditions in the arid eastern pamir. *Catena*, *220*, 106704.

Monge-Salazar, M. J., Tovar, C., Cuadros-Adriazola, J., Baiker, J. R., Montesinos-Tubüe, D. B., Bonnesoeur, V., … Buytaert, W. (2022). Ecohydrology and ecosystem services of a natural and an artificial bofedal wetland in the central andes. *Science of The Total Environment*, *838*, 155968. Retrieved from `https://www.sciencedirect.com/science/article/pii/S0048969722030650` doi: 10.1016/j.scitotenv.2022.155968

Mountain Research Initiative EDW Working Group. (2015). Elevation-dependent warming in mountain regions of the world. *Nature climate change*, *5*(5), 424–430.

Muñoz-Sabater, J., Dutra, E., Agustí-Panareda, A., Albergel, C., Arduini, G., Balsamo, G., … others (2021). Era5-land: A state-of-the-art global reanalysis dataset for land applications. *Earth system science data*, *13*(9), 4349–4383.

Ó Dochartaigh, B. É., MacDonald, A. M., Black, A. R., Everest, J., Wilson, P., Darling, W. G., … Raines, M. (2019). Groundwater–glacier meltwater interaction in proglacial aquifers. *Hydrology and Earth System Sciences*, *23*(11), 4527–4539.

Pfeffer, W. T., Arendt, A. A., Bliss, A., Bolch, T., Cogley, J. G., Gardner, A. S., … others (2014). The randolph glacier inventory: a globally complete inventory of glaciers. *Journal of glaciology*, *60*(221), 537–552.

Polk, M. H., Young, K. R., Baraer, M., Mark, B. G., McKenzie, J. M., Bury, J., & Carey, M. (2017). Exploring hydrologic connections between tropical mountain wetlands and glacier recession in peru's cordillera blanca. *Applied Geography*, *78*, 94–103.

Radić, V., Bliss, A., Beedlow, A. C., Hock, R., Miles, E., & Cogley, J. G. (2014). Regional and global projections of twenty-first century glacier mass changes in response to climate scenarios from global climate models. *Climate Dynamics*, *42*(1), 37–58.

RGI Consortium. (2023). *Randolph glacier inventory (rgi) – a dataset of global glacier outlines, version 7.0.* Boulder, Colorado, USA: NSIDC: National Snow and Ice Data Center. Retrieved from `https://doi.org/10.5067/F6JMOVY5NAVZ` doi: 10.5067/F6JMOVY5NAVZ

Rojas, Y., & Minder, J. R. (2024). Variability of the southern andes rain shadow. *Atmo-*

spheric Research, *308*, 107509.

Ross, A. C., Mendoza, M. M., Drenkhan, F., Montoya, N., Baiker, J. R., Mackay, J. D., … Buytaert, W. (2023). Seasonal water storage and release dynamics of bofedal wetlands in the central andes. *Hydrological processes*, *37*(8), e14940.

Salimi, S., Almuktar, S. A., & Scholz, M. (2021). Impact of climate change on wetland ecosystems: A critical review of experimental wetlands. *Journal of Environmental Management*, *286*, 112160.

Strahler, A. N. (1957). Quantitative analysis of watershed geomorphology. *Eos, Transactions American Geophysical Union*, *38*(6), 913–920.

Taylor, L. S., Quincey, D. J., Smith, M. W., Potter, E. R., Castro, J., & Fyffe, C. L. (2022). Multi-decadal glacier area and mass balance change in the southern peruvian andes. *Frontiers in Earth Science*, *10*, 863933.

Verzijl, A., & Quispe, S. G. (2013). The system nobody sees: irrigated wetland management and alpaca herding in the peruvian andes. *Mountain Research and Development*, *33*(3), 280–293.

White-Nockleby, C., Prieto, M., Yager, K., & Meneses, R. I. (2021). Understanding bofedales as cultural landscapes in the central andes. *Wetlands*, *41*(8), 102.

Wu, Y., Ni, B., Xue, Z., Dong, L., Zhang, K., Rousseau, A. N., … Song, K. (2025). Quantitative assessment of hydrological multifunctionality of headwater wetlands. *Journal of Hydrology*, *657*, 133113.

Zekollari, H., Schuster, L., Maussion, F., Hock, R., Marzeion, B., Rounce, D. R., … others (2025). Glacier preservation doubled by limiting warming to 1.5° c versus 2.7° c. *Science*, *388*(6750), 979–983.

Zemp, M., Frey, H., Gärtner-Roer, I., Nussbaumer, S. U., Hoelzle, M., Paul, F., … others (2015). Historically unprecedented global glacier decline in the early 21st century. *Journal of glaciology*, *61*(228), 745–762.

Supporting Information for

Spatial Patterns of Glacier Meltwater and Mountain Wetland Connectivity in the Peruvian Andes

D. Xuan [1], R. Becker [1] *, M. Vargas Valverde [2], B. Davies [3], J. C. Ely [4], O. King [3], N. Montoya [2], C. Onof [1], A. C. Ross [1], W. Buytaert [1]

[1]Department of Civil and Environmental Engineering, Imperial College London, United Kingdom

[2]Departamento Académico de Agricultura, Universidad Nacional de San Antonio Abad del Cusco (UNSAAC), Cusco, Peru

[3]School of Geography, Politics and Sociology, Newcastle University, Newcastle-upon-Tyne, United Kingdom

[4]School of Geography and Planning, University of Sheffield, Sheffield, United Kingdom

Contents of this file

Introduction

This supporting information provides detailed descriptions of the methodology, additional analyses to enhance the robustness, and supplementary results that support the main conclusions. It includes the wetland mapping approach, sensitivity analyses for flow-accumulation thresholds, a step-by-step glacier dilution workflow, regression coefficients, cross-correlation analyses at different time lags, an explanation of the explained-variance calculation, and relative wetland coverage across sub-catchments at both study sites.

*Corresponding author: R. Becker (r.becker@imperial.ac.uk)

Text S1. Wetland Mapping

Figure S1 displays the wetland mapping framework, which was developed originally to create a global wetland map (see uncertainty assessment results and full mapping code here: https://zenodo.org/records/14930773). For this study, we use the same framework, but only employ it over our two South-Peruvian study regions. Similar to the global map, the wetland maps for this study are created in Google Earth Engine using a supervised classification approach that integrates multiple data sources: i. Spectral information from Sentinel-1 and Sentinel-2 satellite imagery; ii. Topographic information derived from the 30 m NASA SRTM Digital Elevation Model (DEM); and iii. global ecoregion data from the RESOLVE data set (Dinerstein et al., 2017).

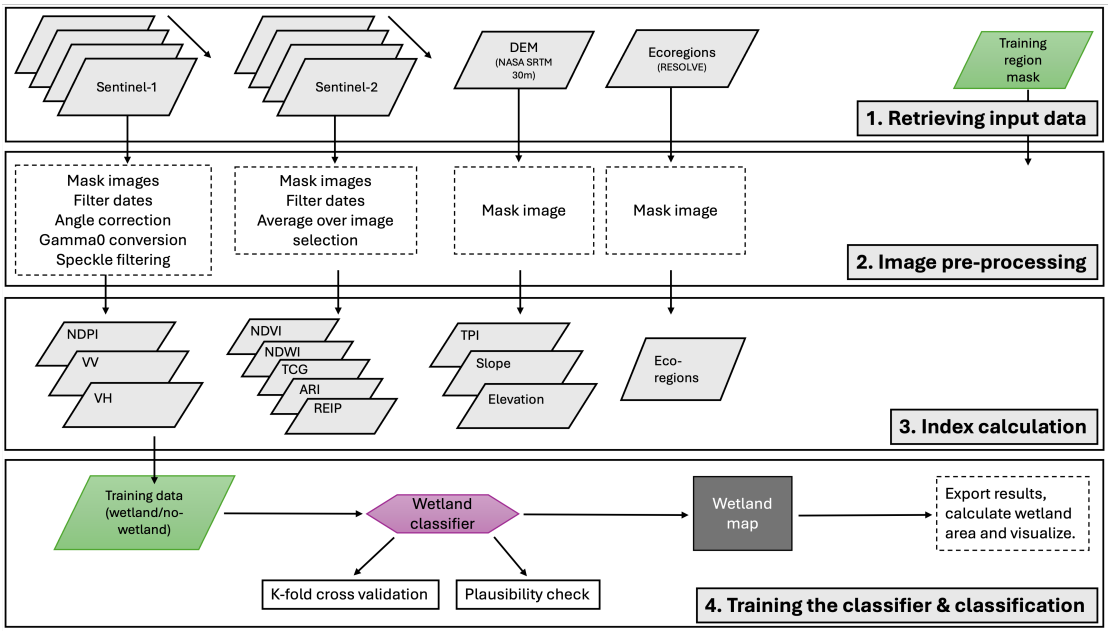

Figure S1. Workflow of the remote-sensing based wetland mapping approach.

Text S2. Sensitivity Analysis

Since the spatial regression is conducted at the sub-catchment scale, it is essential to select an appropriate flow-accumulation (facc) threshold for delineating sub-catchments from the Digital Elevation Model (DEM). The facc threshold represents the minimum number of contributing cells required to initiate a stream and delineate river networks. This value is region-specific, difficult to determine, and requires careful consideration (López-Vicente et al., 2014; Zhang et al., 2021).

In this study, we performed a sensitivity analysis to evaluate flow-accumulation thresholds of 1,000, 2,000, 5,000, and 8,000 cells, examining how these thresholds influence the classification of distance groups and how the mean wetland extent fraction varies across groups under different threshold settings.

S2.1 North: Cordillera Vilcanota region

Different facc thresholds determine the size of each sub-catchment, thereby affecting the total coverage of each distance group (Figure S2a-d). The overall geospatial patterns and relative positions among groups remain similar regardless of the threshold value. However, the choice of threshold has little impact on the relationship of mean wetland extent fraction among the three distance groups (Figure S2e-h): the far-distance group consistently shows higher wetland fractions during wet seasons across years. Sub-catchments closer to glaciers exhibit the least variability in wetland extent. Thus, this distance-dependent relationship is largely insensitive to the facc threshold.

As for which threshold to adopt, a higher facc value results in larger sub-catchments, since more drainage cells are required to form a catchment, thereby covering a greater area. Conversely, if the sub-catchment size is too small (e.g., facc = 1,000; Figure S2a), the wetland areas within each catchment become limited, increasing uncertainty in wetland classification—potentially leading to misclassifications that could distort observed wetland dynamics in an individual sub-catchment. On the other hand, if the sub-catchments are

too big (e.g., facc = 8,000; Figure S2d), the difference between far- and medium-distance groups becomes exaggerated.

Given that wetland fraction dynamics are relatively insensitive to the facc threshold, we adopted a 5,000-cell threshold for its balance between computational efficiency and spatial robustness. Stream networks in all regions were delineated using this uniform threshold, meaning that only cells receiving runoff from at least 5,000 upstream cells were classified as river channels.

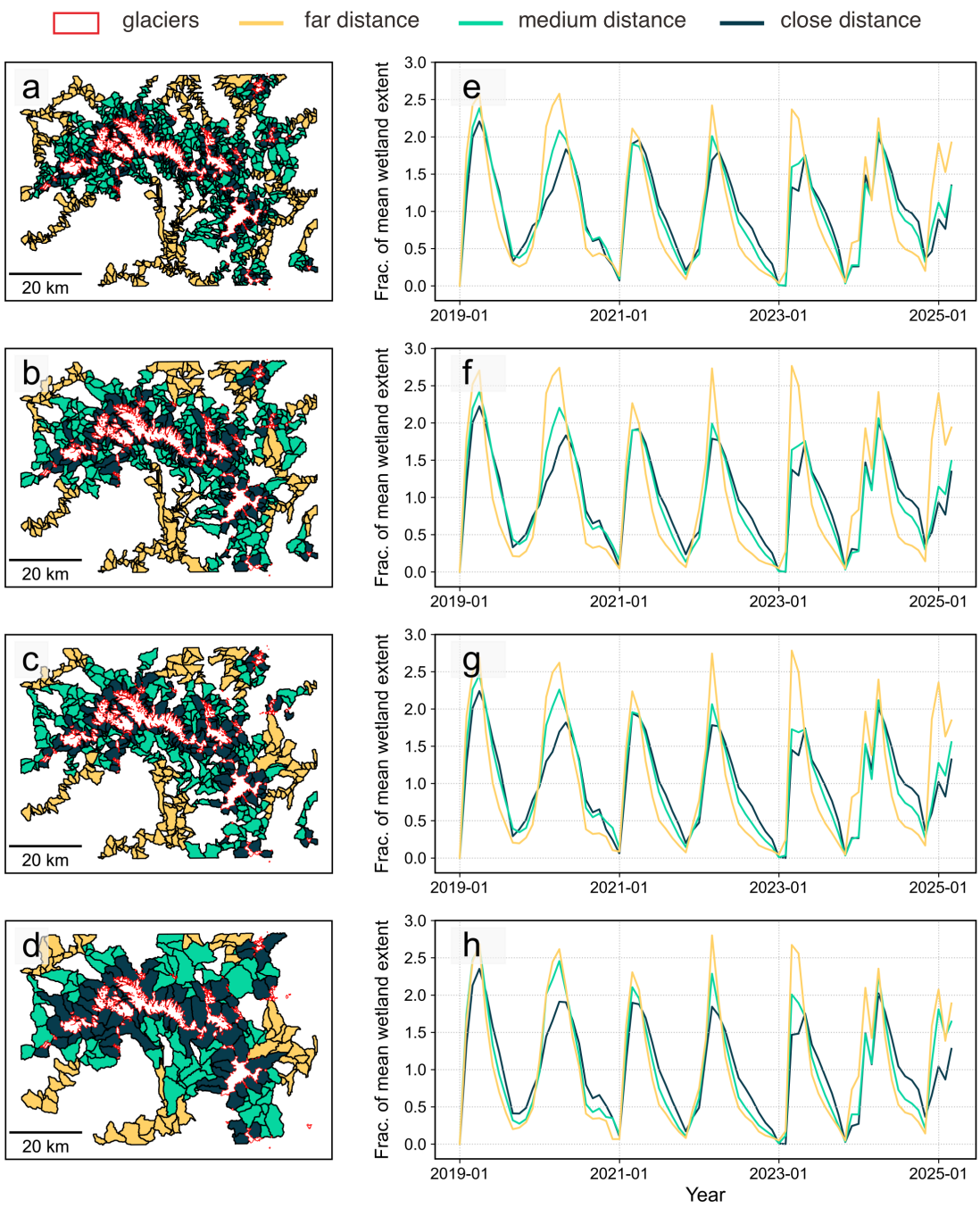

Figure S2. Sensitivity analysis of flow accumulation (facc) thresholds in sub-catchment delineation within the Cordillera vilcanota region. (a-d) Geospatial distribution for sub-catchments for different distance groups. (e-h) Fraction of mean wetland extent across distance groups. Each row corresponds to facc threshods of 1000, 2000, 5000, and 8000, respectively.

S2.2 South: La Raya region

The overall conclusion of the sensitivity analysis in the La Raya region is consistent with that in the Cordillera Vilcanota region: larger facc values produce larger sub-catchments that cover wider areas; whereas smaller thresholds generate smaller sub-catchments and may introduce greater uncertainty, especially when the baseline wetland coverage within an individual sub-catchment is minimal (Figure S3a-d).

In the southern region, the relationship among the three distance groups is less consistent across different facc thresholds, with facc = 1,000 and 2,000 showing similar patterns (Figure S3e-f). Overall, the differences among groups are smaller. The wetland variability in the far-distance group is no longer the most pronounced; instead, the close-distance group exhibits the highest wetland fraction from 2021 onward. However, this higher variability could stem from the small size and limited coverage of the close-distance group. When the threshold increases beyond 5,000, the relationship changes slightly. The wetland fractions remain highest from 2019 to 2021 and in 2024, while being nearly identical during the other years. This change probably because more sub-catchments were classified in the close-distance group as the facc value increases (Figure S3g-h).

In summary, the wetland dynamics across distance groups in the La Raya region differ from those in the Vilcanota region. Areas closer to glaciers no longer show consistently higher wetland fractions throughout the year; instead, the dynamics become more similar among groups.

To avoid overemphasizing the apparent variability in groups with small sample sizes and to enable a more direct comparison between the two regions, we adopted the same facc threshold for the La Raya region as used for the Cordillera Vilcanota region.

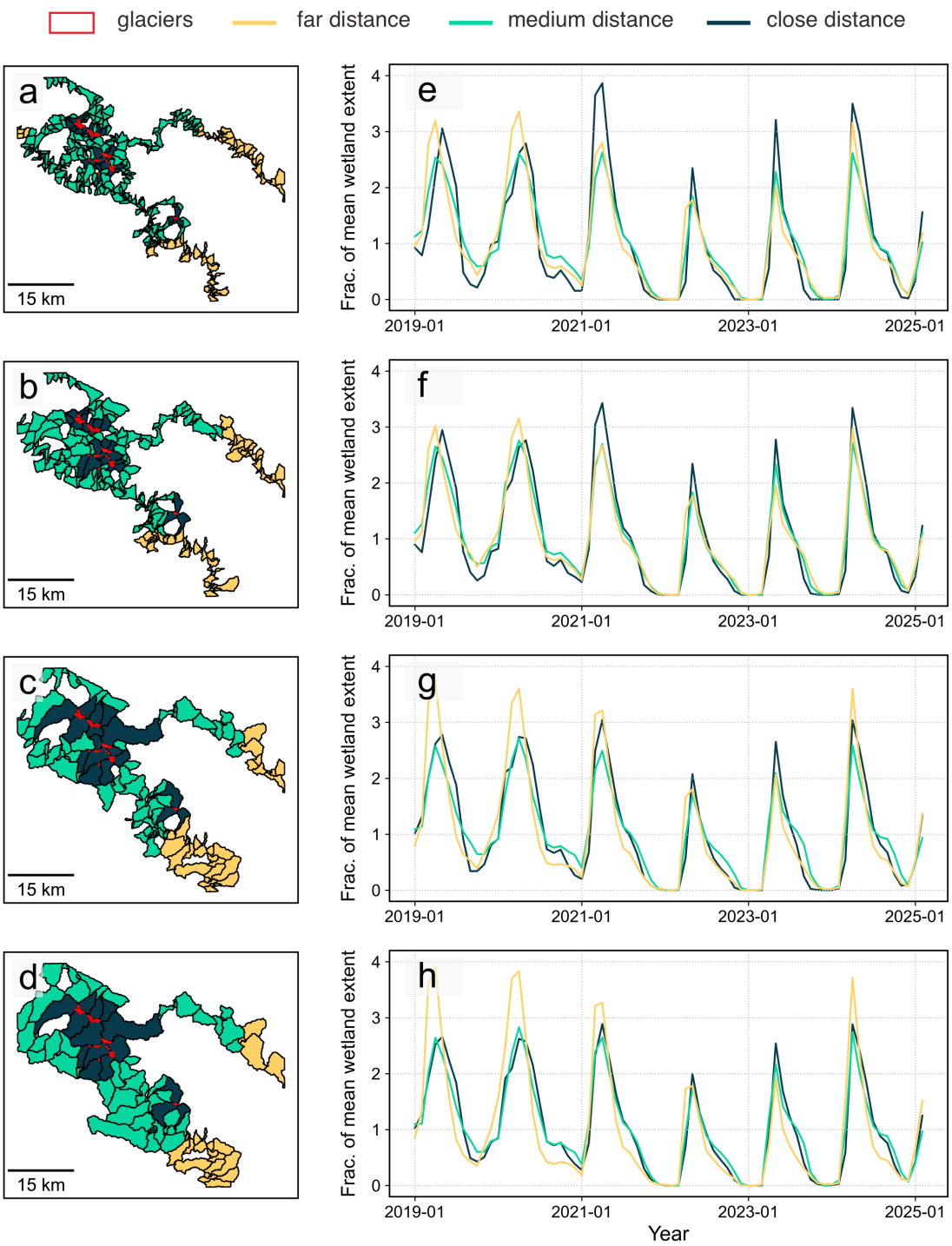

Figure S3. Sensitivity analysis of flow accumulation (facc) thresholds in sub-catchment delineation within the La Raya region. (a-d) Geospatial distribution for sub-catchments for different distance groups. (e-h) Fraction of mean wetland extent across distance groups. Each row corresponds to facc threshods of 1000, 2000, 5000, and 8000, respectively.

Text S3. Glacier Dilution Algorithm

We assumed that the glacier impacts on high mountain wetlands propagate to each sub-catchment through stream networks delineated using the facc value of 5,000 cells. Three flags were defined to quantify glacial impacts for each segment:

1. ***glacier_flag***: Assigned once at the outset, this binary indicator equals 1 if the segment intersects a directly impacted sub-catchments (i.e., close-distance group) and 0 otherwise. It remains constant throughout propagation.

2. ***cum_flag***: Indicates the cumulative upstream glacier impact. A value of 1 indicates direct glacial impact, while 0 denotes no upstream glacial influence. Other values larger than 1 reflect diluted glacial impacts. The higher the value, the greater the dilution effect.

3. ***inflow_count***: For a given segment, this records the number of upstream tributaries whose *cum_flag* is zero (i.e., glacier-unfed tributaries).

The *glacier_flag* serves as a constant initial condition for each stream segment. Propagation then proceeds in ascending Strahler Order and flow accumulation. For first-order segments, which do not have any upstream tributaries, *inflow_count* = 0 and *cum_flag* = *glacier_flag*. For segments of order n (where $n \geq 2$), the downstream flags are derived exclusively from their immediate upstream tributaries as follows:

1. Create a list of *cum_flag* values from all directly converging tributaries.

2. Compute downstream *inflow_count* = number of zeros in that list.

3. If `max`(upstream *cum_flag*) = 0, then downstream *cum_flag* = 0; otherwise, *cum_flag* = `max`(upstream *cum_flag*) + *inflow_count*.

This procedure ensures that each segment's *cum_flag* captures the greatest dilution effect of glacial influence upstream. Once all stream segments have updated their flag values, each sub-catchment inherits the *cum_flag* from its longest intersecting segment. The flowchart of this algorithm presented as pseudocode is shown in Figure S4. The methodology and

rationale underlying the classification of each distance group are presented in the main text.

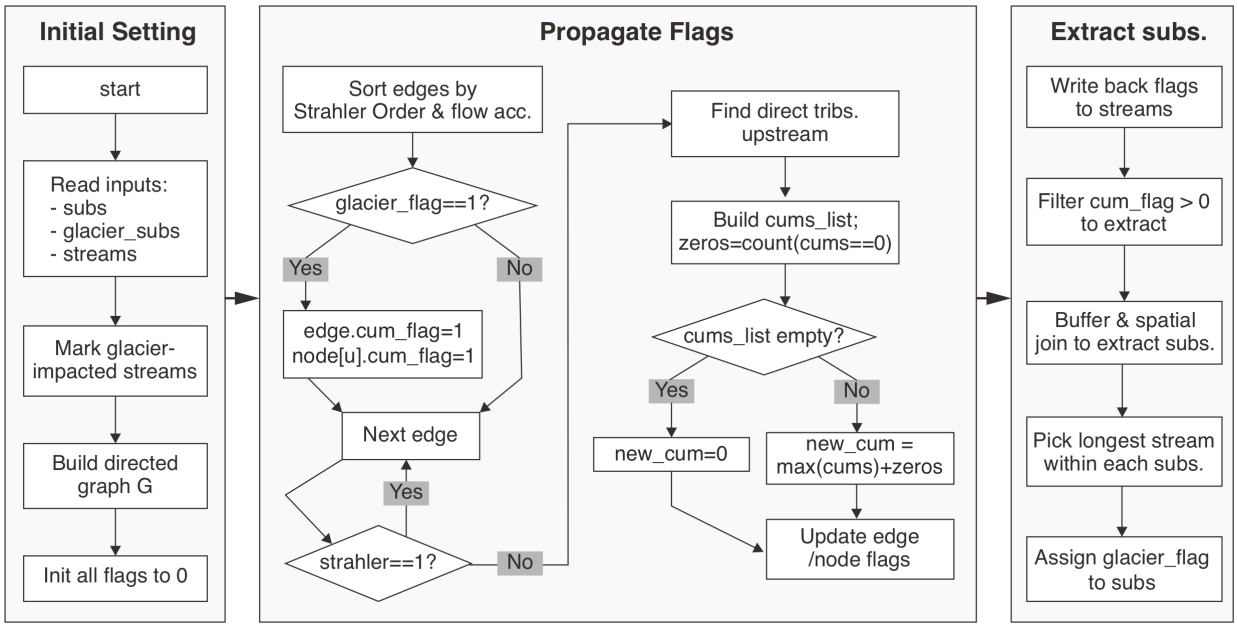

Figure S4. The workflow of propagating glacier's dilution impacts.

Text S4. Spearman correlation

Spearman correlation (ρ_s), which relies on the ordinal ranking of observations rather than their raw values, is appropriate when the assumptions underlying Pearson's correlation are violated (Gogtay & Thatte, 2017). Before calculating Spearman's correlation, the paired observations (X_i, Y_i) are first sorted, then ranked and denoted ($R(X_i)$, $R(Y_i)$). The equations are shown as below:

$$\rho_s = 1 - \frac{6 \sum_{i=1}^{n} d_i^2}{n(n^2 - 1)} \tag{1}$$

where $d_i = R(X_i) - R(Y_i)$ is the difference in ranks for ith pair; ρ_s is the Spearman rank correlation coefficient; n is the number of paired observations.

We calculated the Spearman correlation between the regional average time series of wetland extent, temperature, and precipitation. To identify the most appropriate lag between wetland dynamics and climatic predictors, we applied cross-correlation analysis. Because wetlands respond to local climate with a delay due to runoff accumulation and hydrological buffering, we shifted the wetland time series from no lag up to 4-month lag relative to temperature and precipitation. Spearman correlations were then computed for each lagged wetland series against the climatic predictors. In the Cordillera Vilcanota region, we found that a 3-month lag produced the strongest and most significant correlation. For consistency and to enable direct comparison, we applied this same lag to the southern study site.

Text S5. Ridge regression coefficients

Table S1. The average coefficients and its corresponding 95 % confident intervals (CI) across distance groups in two study sites.

Study site	Distance to glaciers	Variables			
		temperature	*precipitation*	*seasonality*	*trend*
Cordillera Vilcanota	far dist.	0.02 ± 0.04	0.26 ± 0.09	0.27 ± 0.08	-0.07 ± 0.03
	medium dist.	0.04 ± 0.04	0.21 ± 0.04	0.21 ± 0.04	-0.11 ± 0.04
	close dist.	0.02 ± 0.03	0.14 ± 0.05	0.14 ± 0.03	-0.04 ± 0.03
La Raya	far dist.	/	0.26 ± 0.08	0.20 ± 0.06	-0.14 ± 0.05
	medium dist.	/	0.14 ± 0.03	0.18 ± 0.05	-0.09 ± 0.02
	close dist.	/	0.27 ± 0.30	0.32 ± 0.30	-0.18 ± 0.24

Text S6. Explained Variance Calculation

Apart from using standardized regression coefficients to compare predictors across sub-catchments, we quantify the explained variance to assess the relative importance of each predictor within individual sub-catchments (Grömping, 2007). This metric reflects how strongly the contribution of a given predictor varies together with the overall model prediction. Predictors whose contributions are closely aligned with the predicted response account for a larger share of the explained variance.

In our Ridge linear regression model, let $\hat{y}_c = \hat{y} - \mathbb{E}[\hat{y}]$ denote the centered model prediction, which can be written as the sum of the individual predictor contributions:

$$\hat{y}_c = \sum_j X_j \beta_j \tag{2}$$

The total explained variance of the model is quantified by the coefficient of determination,

$$R^2 = \frac{\mathrm{Var}(\hat{y}_c)}{\mathrm{Var}(y)} \tag{3}$$

which measures how much of the variability in the observed response is captured by the model prediction, and where $\mathrm{Var}(y)$ denotes the variance of the observed response within each sub-catchment. Because the model prediction is the sum of predictor-specific contributions, the variance of the prediction can be decomposed using the linearity of covariance:

$$\mathrm{Var}(\hat{y}_c) = \sum_j \mathrm{Cov}(X_j \beta_j, \hat{y}_c) \tag{4}$$

Based on this, the fraction of explained variance attributed to predictor j was defined as:

$$w_j = \frac{\mathrm{Cov}(X_j \beta_j, \hat{y}_c)}{\mathrm{Var}(y)} \tag{5}$$

By construction, the predictor-specific contributions sum exactly to the model R^2:

$$\sum_j w_j = R^2 \tag{6}$$

Text S7. Relative wetland coverage

Relative wetland coverage is calculated as the ratio of wetland area within each sub-catchment to the total sub-catchment area.

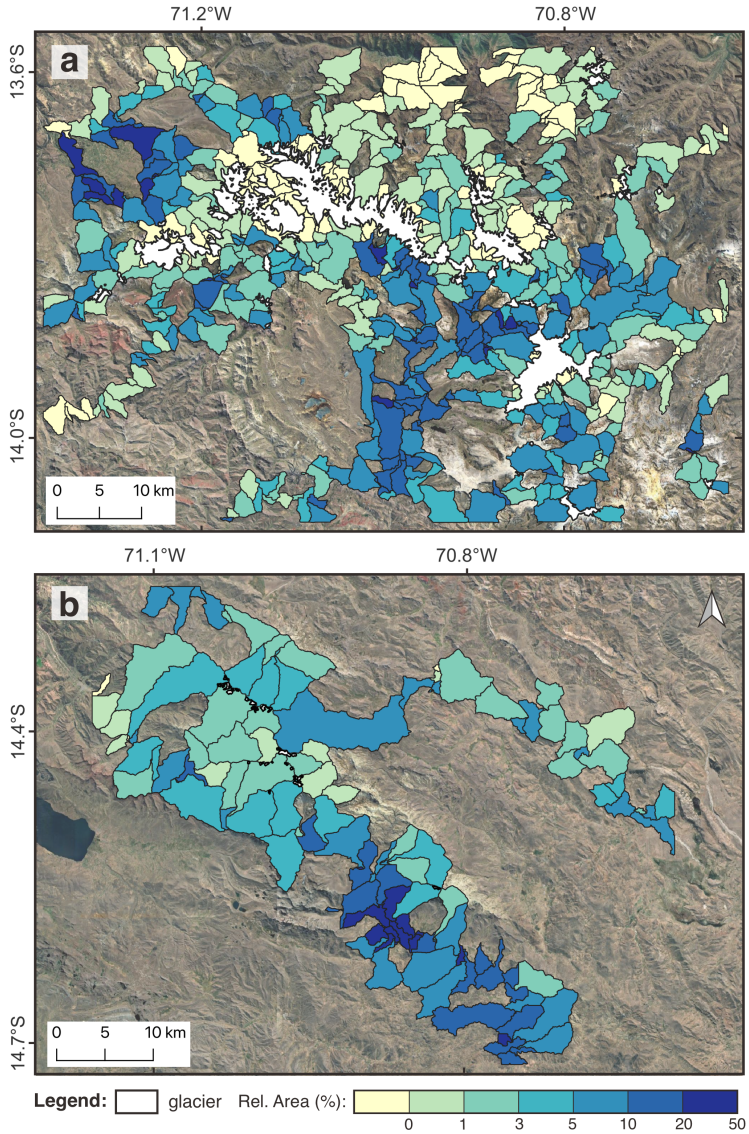

Figure S5. The relative wetland area per sub-catchment in the Cordillera vilcanota region (a) and La Raya region (b) within three distance groups.

References

Dinerstein, E., Olson, D., Joshi, A., Vynne, C., Burgess, N. D., Wikramanayake, E., … others (2017). An ecoregion-based approach to protecting half the terrestrial realm. *BioScience*, *67*(6), 534–545.

Gogtay, N. J., & Thatte, U. M. (2017). Principles of correlation analysis. *Journal of the Association of Physicians of India*, *65*(3), 78–81.

Grömping, U. (2007). Estimators of relative importance in linear regression based on variance decomposition. *The American Statistician*, *61*(2), 139–147.

López-Vicente, M., Pérez-Bielsa, C., López-Montero, T., Lambán, L. J., & Navas, A. (2014). Runoff simulation with eight different flow accumulation algorithms: Recommendations using a spatially distributed and open-source model. *Environmental Modelling & Software*, *62*, 11–21.

Zhang, W., Li, W., Loaiciga, H. A., Liu, X., Liu, S., Zheng, S., & Zhang, H. (2021). Adaptive determination of the flow accumulation threshold for extracting drainage networks from dems. *Remote Sensing*, *13*(11), 2024.